Progress In Electromagnetics Research C, Vol. 66, 173–182, 2016

A CPW-Fed Microstrip Fork-Shaped Antenna with Dual-Band Circular Polarization

Chien-Jen Wang and Yu-Wei Cheng*

Abstract—This paper presents a microstrip wideband antenna and its utilization in integration of multiple wireless communication systems. A simple fork-like strip antenna, fed by a coplanar-waveguide (CPW) transmission line, is designed to excite a right-hand circularly polarized wave at 1.57 GHz. A rectangular patch is added at the end of one prong to enhance the circular polarization performance. By modifying the geometry of the ground plane, a left-hand circularly polarized wave is excited at 2.33 GHz, and the wideband frequency response is derived. To reduce the lower resonant frequency, a stub is added at the left side of the ground plane. The measured impedance bandwidth of reflection coefficients (S_{11}) < -10 dB ranges from 1.49 to 2.92 GHz, which satisfies the system bandwidths of most of commercial wireless communication systems. The 3-dB axial-ratio bandwidths are approximately 40 MHz at the lower band (1.57 GHz) and 290 MHz at the upper band (2.33 GHz).

1. INTRODUCTION

The circularly polarized antenna has attracted much attention owing to the applications in global positioning system, satellite digital audio radio, radio frequency identification (RFID), etc. presently. Compared with a linearly polarized wave, a radiating wave with the circular polarization (CP) can provide improved gain and cross-polar discrimination so that the effect of multi-path interference, which produces fading, can be reduced. In recent years, the fast development of multi-system integration technology has initialized growing interest in dual-band circularly polarized antenna. Some dual-band circularly polarized antennas have been investigated and presented, such as the patch [1, 2] or the slot [3, 4]. For example, an S-shaped slotted patch antenna with dual-band CP has been presented for GPS applications [1]. The asymmetrical S-shaped slot, which acts as a perturbation of the patch, excites the two orthogonal field components with a 90° phase-shift for the CP operation at the lower frequency band. In addition, by adjusting the geometry of the S-shaped slot, CP at the upper frequency band is also generated. In [3], the dual-band performance with right-hand circular polarization (RHCP) for the lower frequency and the left-hand circular polarization (LHCP) for the upper frequency has been realized by utilizing a spiral slot. The AR bandwidth is improved by embedding an additional spiral slot inside the dominant slot radiator.

Because of simple structure, small size, broad impedance bandwidth, light weight, good radiation efficiency, and easy impedance matching, some types of the printed monopole antenna have been developed. Some designs of the dual-frequency monopole antenna have been reported in [5–8]. In [5], a two-finger monopole achieves dual-band performance, and the performance is easily tuned by changing the finger length, individually. For WLAN 2.4/5.2 dual-band operations, a CPW-fed inverted-L monopole antenna has been presented [6]. It is seen that the radiation patterns of the proposed antenna are monopole-like. Some studies about the circularly polarized monopole antenna have been presented [9–12]. In 2008, we added an inverted-L sleeve at the ground plane of the C-like monopole,

Received 22 May 2016, Accepted 28 July 2016, Scheduled 8 August 2016
* Corresponding author: Yu-Wei Cheng (goodluck0621@gmail.com).
The authors are with the Department of Electrical Engineering, National University of Tainan, Taiwan.

and the CP excites [9]. A loop-like monopole antenna with CP has been shown in [10]. By utilizing a two-loop technology with an asymmetrical feeding structure, the antenna can not only provide the wide impedance bandwidth, but the AR bandwidth also reaches about 12%. In 2014, a CPW-fed circularly polarized monopole antenna for multiple system integration has been developed [12]. To excite the CP at 1.57 GHz, an asymmetrical ground plane was used.

The dual-band CP for the monopole has been noticed owing to its attractive feature, which covers two wireless communication systems with required CP performance, such as GPS, SDAR, or WLAN. A first work of the dual-band CP for the monopole antenna has been shown in 2009 [13]. The design of a modified monopole with a slotted ground plane can excite dual-band circularly polarized radiation waves. The 3-dB axial-ratio bandwidths are about 150 MHz at 2.5 GHz and 230 MHz at 3.4 GHz. Another dual-band CP design for applications of 2.4/5.2-GHz WLAN systems has been introduced in [14]. The proposed antenna consists of an F-like monopole and an inverted-L grounded strip. It is noted that the locations of the dual circularly polarized bands are difficult to control in the previous works.

In this paper, a broadband monopole antenna with dual-band circular polarization is demonstrated. Techniques for achieving CP are introduced, and a new CP mechanism is proposed. A quasi-dipole resonant mode is generated along a two-prong fork-like monopole, where a half-wavelength dominates resonance. This mode along the monopole results in the lower resonant impedance band and a RHCP excitation at 1.57 GHz. Furthermore, by decreasing the size of one side of the ground plane, another quasi-dipole mode is also excited along the monopole and the ground plane. The upper resonance and a wave with LHCP at 2.33 GHz are attributed to the second quasi-dipole mode. For understanding of the operation principle for resonance excitation and dual-band CP, the current distributions are presented.

2. ANTENNA DESIGN

A geometrical diagram of the proposed monopole antenna with dual-band CP is shown in Fig. 1. Table 1 lists the dimensional parameters of the proposed antenna after the optimization process. The proposed antenna is fabricated on an FR4 microwave substrate with a thickness of 1.6 mm, relative permittivity of 4.4 and loss tangent of 0.02. The prototype was derived from a two-prong fork shape. The length of each prong is determined by a quarter-wavelength. A rectangular patch is connected at the end of the long prong, which decides the lower frequency band around 1.57 GHz. The length of the short prong is designed with respect to the operated frequency of 2.0 GHz. By reducing the length of the right side of the ground plane the unbalanced situation of the horizontal currents along the two sides of the ground plane is achieved. To solve the problem of the poor impedance matching condition, the width of the left side of the ground plane increases. Finally, a stub is added at the left side of the ground plane for frequency decrease at the lower frequency band. Fig. 2 shows the design evolution of the proposed CPW-fed monopole antenna with dual-band CP. Prototype is a conventional CPW-fed monopole antenna with a two-prong fork-like topology. Antenna 1 is a prototype with a rectangular-path loading. After cutting part of the right side of the ground plane, the case is denoted by Antenna 2. Antenna 3 is the structure of Antenna 2 with an extended width of the ground plane. Antenna 3 with the grounded stub is denoted by Proposed.

Table 1. Geometrical parameters of the proposed monopole antenna.

Parameter	L_{m1}	L_{m2}	L_f	L_t
Unit (mm)	21.3	6	18	2.5
Parameter	L_{s1}	L_{s2}	W_{s1}	W_{s2}
Unit (mm)	13	28.5	16	32
Parameter	W_f	W_{m1}	W_{m2}	W_{m3}
Unit (mm)	6.34	1	1	7.4
Parameter	W_d	W_t	g_1	g_2
Unit (mm)	2	2	0.5	1.7

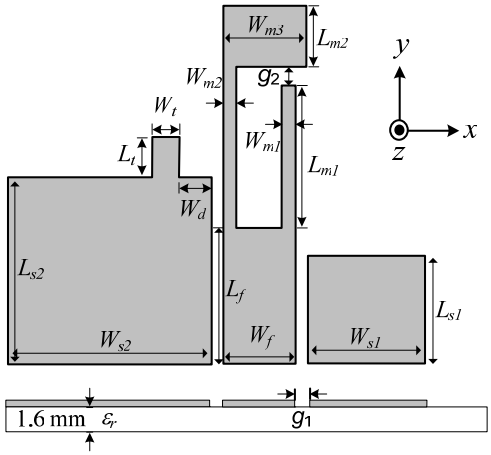

Figure 1. Schematic configuration of the proposed CPW-fed fork-shaped antenna.

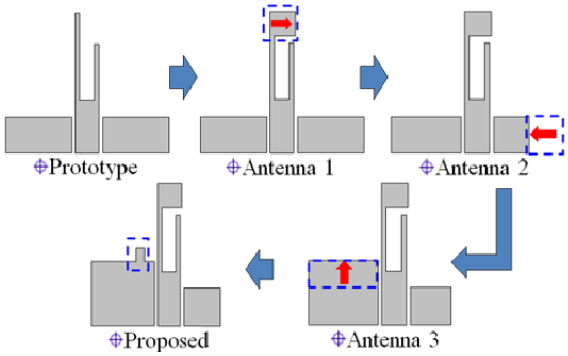

Figure 2. Design evolution of the proposed CPW-fed monopole antenna.

3. RESULTS AND DISCUSSION

All of CPW-fed monopole antennas in this experiment were simulated by using the EM software Ansys high frequency structure simulator (HFSS). With the assistance of this software, the expected performance of the antenna is fully constructed, especially over the operated frequency band. Fig. 3 shows comparisons of the simulated reflection coefficient and axial ratio of several specified antennas, including Prototype, Antenna 1, Antenna 2, and Antenna 3. The AR results are measured in the $+z$-direction. For the Prototype case, there are two resonant modes around 1.67 and 2.06 GHz, which are dominated by the quarter wavelength of the two prongs. Due to the strong standing wave along the two prongs, the radiating wave is linearly polarized, and thus the AR is large.

For Antenna 1, after adding the rectangular patch at the end of the long prong, the impedance characteristics show that the resonant frequency of the lower operated band shifts downward with a slight variation in the upper operated band. The AR performance improves because of the existence of

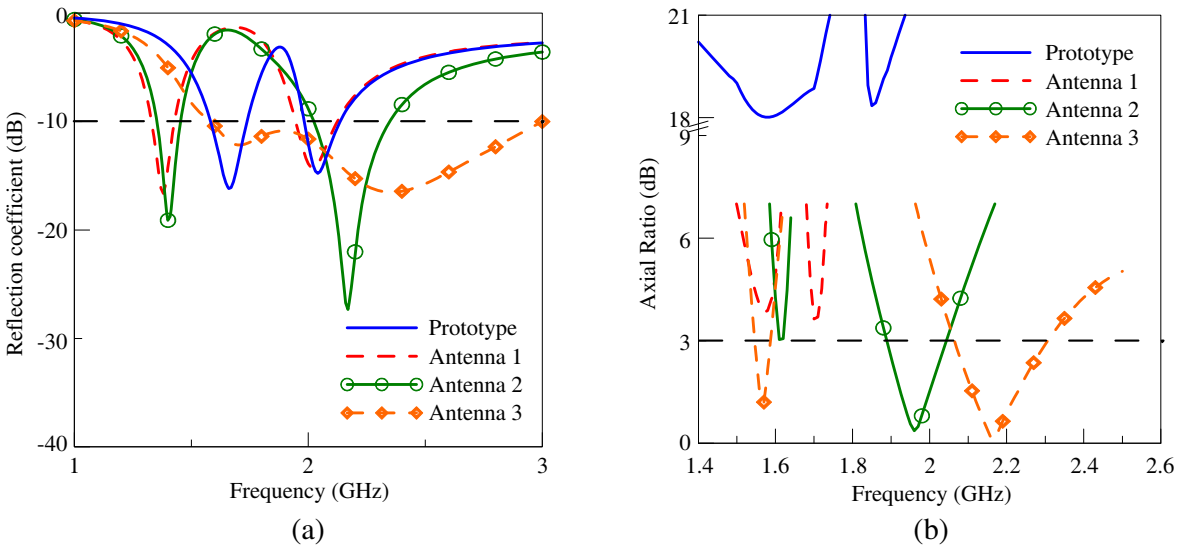

Figure 3. Simulated curves of the reflection coefficient and axial ratio of four types of the monopole antenna. (a) Reflection coefficient. (b) Axial ratio.

the horizontal current at the stub. Utilization of reducing the size of the left-side ground plane not only reduces the occupied area of Antenna 2, but also improves the bandwidth and impedance matching condition. Moreover, because of the enhancement of the horizontal current along the ground-plane edges, the AR characteristics show an effective improvement, particularly around the upper operated frequency. The unbalanced ground-plane topology results in the excitation of a new electrical field orthogonal to the monopole-induced electrical field. Antenna 3, for which the left-side width of the ground plane increases, exhibits dual-resonance operation with a band ranging from 1.58 to 2.99 GHz. The merging of two resonances achieves a broader bandwidth. Although well-matched DCS, PCS, IMT-2000, WLAN, and LTE2600 bands are observed, the impedance bandwidth around the 1.57-GHz region (for GPS) is mismatched. As revealed in the AR results of Fig. 3(b), dual-band CP is achieved.

Figure 4 shows a comparison of the simulated S_{11} and AR of Antenna 3 with and without the grounded stub. In the proposed antenna design, after adding the grounded stub, the matching condition in the lower operated band, which is controlled by the long prong monopole, effectively improves, resulting in increased impedance bandwidth. The band requirement of the GPS system is satisfied. Furthermore, the CP results in Fig. 4(b) show that the minimum value of the axial ratio at the upper band shifts to a higher frequency. The measured S_{11} and AR of the proposed antenna are also shown in Fig. 4. The measured impedance bandwidth for a 10-dB reflection coefficient is 1.49–2.92 GHz (a 1.43-

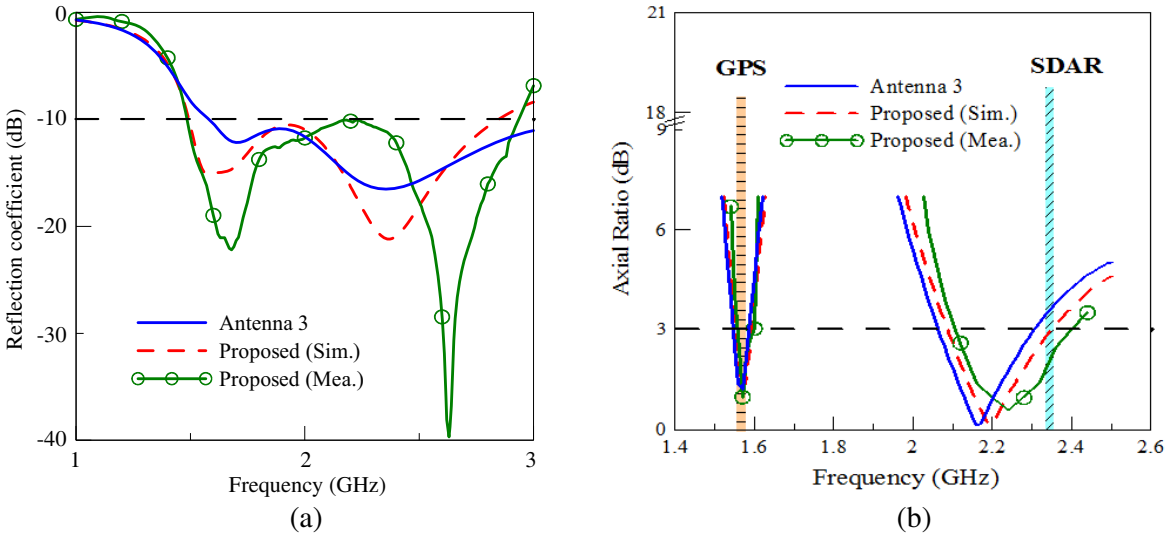

Figure 4. Simulated curves of the reflection coefficient and axial ratio of the Antenna 3 with and without the grounded stub. (a) Reflection coefficient. (b) Axial ratio.

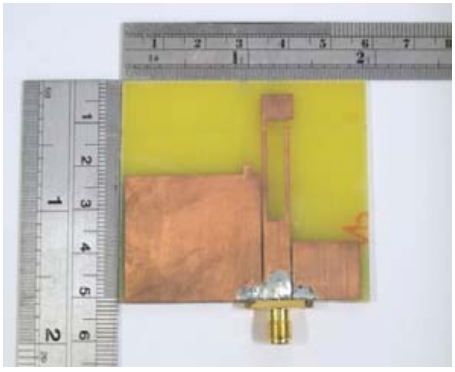

Figure 5. Photographs of the fabricate monopole antenna.

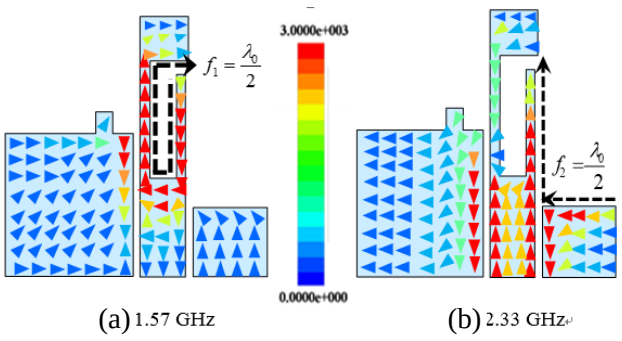

Figure 6. Simulated current density distributions of the proposed antenna.

Table 2. Comparison of some past studies and our work.

Parameter \ Reference	**Proposed**	**[13]**	**[15]**
Total size (mm ∗ mm ∗ mm)	55.3 ∗ 47 ∗ 1.6	40 ∗ 39 ∗ 1.6	30 ∗ 60 ∗ 1.6
Impedance BW (−10 dB, MHz, %)	1.49 ∼ 2.92 GHz (1430 MHz, 64.9%)	2.17–8.47 GHz (6300 MHz, 118.4%)	2.42–2.51 GHz (85 MHz, 3.4%) 5.26–5.50 GHz (240 MHz, 4.5%)
Axial ratio BW (−3 dB, MHz, %)	1.56 ∼ 1.60 GHz (40 MHz, 2.5%) 2.11 ∼ 2.40 GHz (290 MHz, 12.9%)	2.41–2.55 GHz (140 MHz, 5.6%) 3.45–4.35 GHz (900 MHz, 23.1%)	2.42–2.47 GHz (50 MHz, 2.0%) 5.28–5.35 GHz (75 MHz, 1.4%)
Parameter \ Reference	**[16]**	**[14]**	-
Total size (mm ∗ mm ∗ mm)	30 ∗ 30 ∗ 1.6	40 ∗ 45 ∗ 1.6	-
Impedance BW (−10 dB, MHz, %)	1.50–2.50 GHz (1000 MHz, 50.0%) 4.70–5.83 GHz (1140 MHz, 21.7%)	1.92–3.85 GHz (193 MHz, 67.0%) 5.12–5.46 GHz (340 MHz, 6.4%)	-
Axial ratio BW (−3 dB, MHz, %)	1.50–2.09 GHz (590 MHz, 33.1%) 4.71–5.33 GHz (620 MHz, 11.8%)	2.27–2.52 GHz (250 MHz, 10.4%) 5.11–5.47 GHz (360 MHz, 6.8%)	-

GHz impedance bandwidth; 69.4%), whereas the simulated impedance bandwidth is 1.50–2.84 GHz (a 1.34-GHz bandwidth; 61.8%). The shift maybe comes from fabrication tolerances and material parameter uncertainty. The measured 3-dB AR bandwidths at the lower and upper bands are 2.5% (1.56–1.60 GHz; 1.58 GHz) and 12.9% (2.11–2.40 GHz; 2.255 GHz), respectively; both satisfy the −10-dB S_{11} bandwidth threshold. Fig. 5 shows a photograph of a fabricated antenna after optimum process. A comparison of some past studies [13–16] and our work for the dual-band circular polarization is shown in Table 2. Note that all of the references in the table are designed by the monopole antenna. Compared with other referenced studies, the most attractive performance of the proposed monopole antenna is that the impedance bandwidth covers the system bandwidths of the commercial wireless communication systems, such as GPS (at 1.57 GHz), DCS (at 1.8 GHz), PCS (at 1.9 GHz), IMT-2000 (at 2.1 GHz), SDAR (at 2.33 GHz), WLAN (at 2.4 GHz), and LTE2600 (at 2.6 GHz). In addition, the proposed antenna with circular polarization achieved at the 1.57 and 2.33 GHz can be utilized in the GPS and SDAR applications. It makes the proposed antenna a candidate for multi-integration applications of wireless communication systems.

Figure 6 presents the simulated surface current density distributions of the proposed antenna. According to the results, the 1.57- and 2.33-GHz modes are mainly induced with current paths of approximately 0.37 and 0.33 wavelengths corresponding to the operated frequency. For 1.57-GHz band excitation, according to the current distribution, the resonant path is the two-prong monopole because the electric currents on the two prongs are quasi-symmetrical and reach zero at the ends. The shape of the current distribution is a bent quasi-dipole. For 2.33-GHz band excitation, the short prong strip and the ground plane are simultaneously excited instead of only the monopole path. Figs. 7 and 8 reveal the current distributions at the CP frequencies of 1.57 and 2.21 GHz. Notably, in Fig. 8, the CP frequency with the minimum AR in the lower band is that of the first resonance in the impedance

characteristics. The CP at 1.57 GHz is caused by the alternate excitation of the conductor components of the two prongs. The mechanism of the single-mode CP is similar to that of the CP in the form of the traveling-wave mode. The simulated surface current components rotate anticlockwise, thus yielding a wave with RHCP in the $+z$ direction. The simulated results in Fig. 8 suggest that, because of the radiation of the quasi-dipole mode around 2.21 GHz, the induced current distributes along the short prong strip and the right-side edge of the ground plane. The currents at 2.21 GHz rotate clockwise, thus generating a wave with LHCP.

Figure 9 shows the simulated and measured radiation patterns of the proposed monopole antenna at three operating frequencies (1.8, 2.1, and 2.6 GHz) utilized in the DCS, IMT-2000, and LTE 2600

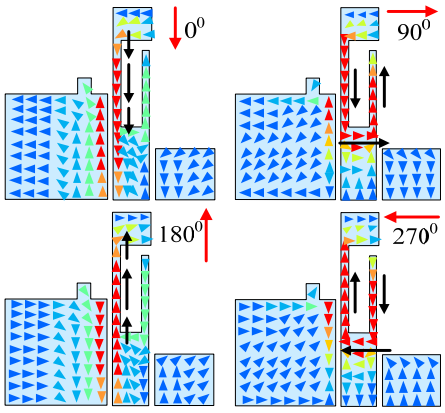

Figure 7. Current distributions of the proposed antenna for the CP frequency of 1.57 GHz.

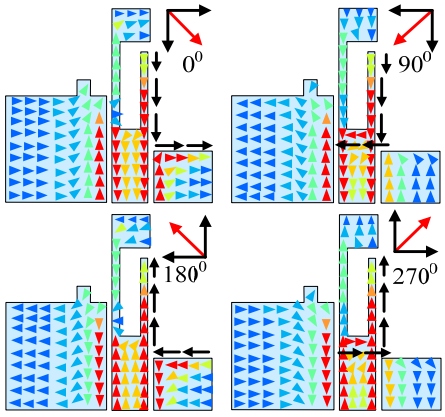

Figure 8. Current distributions of the proposed antenna for the CP frequency of 2.21 GHz.

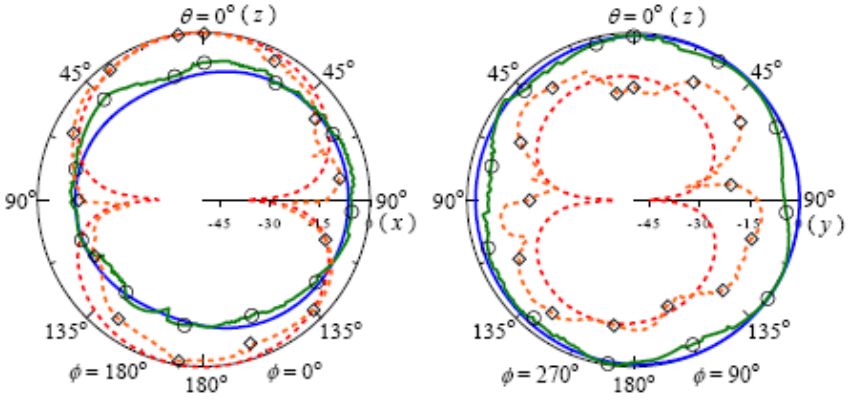

(a)

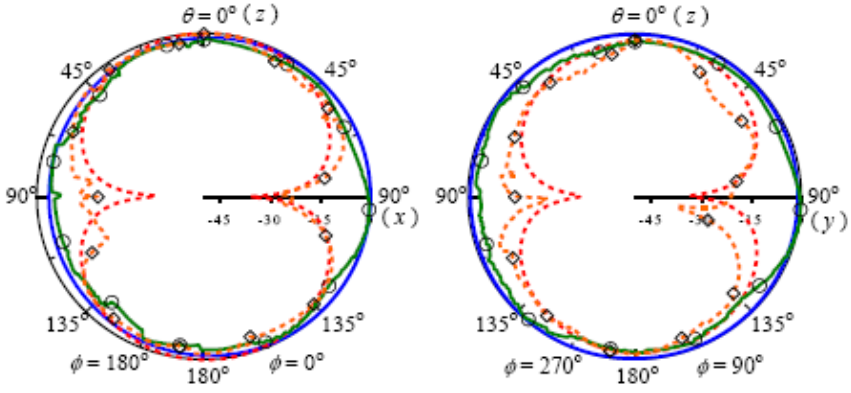

(b)

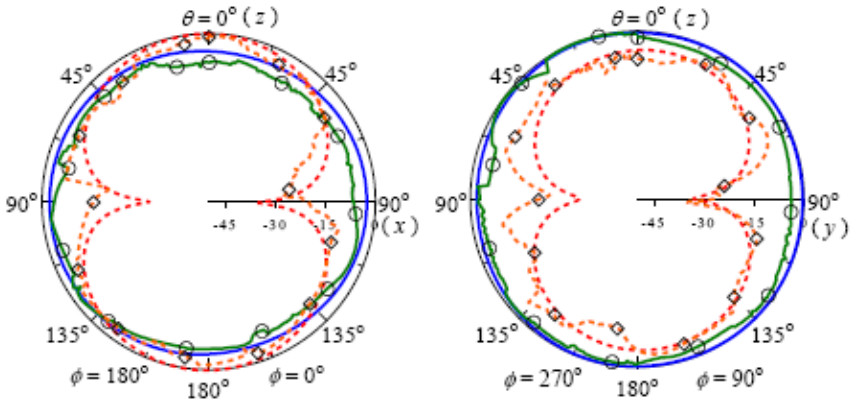

(c)

Figure 9. Simulated and measured radiation patterns of the proposed antenna at 1.8, 2.1, and 2.6 GHz. The EM simulator-achieved results are shown as the blue solid line and red dashed line, when the measured values are shown as the green line and orange line with symbols. (a) 1.8 GHz. (b) 2.1 GHz. (c) 2.6 GHz.

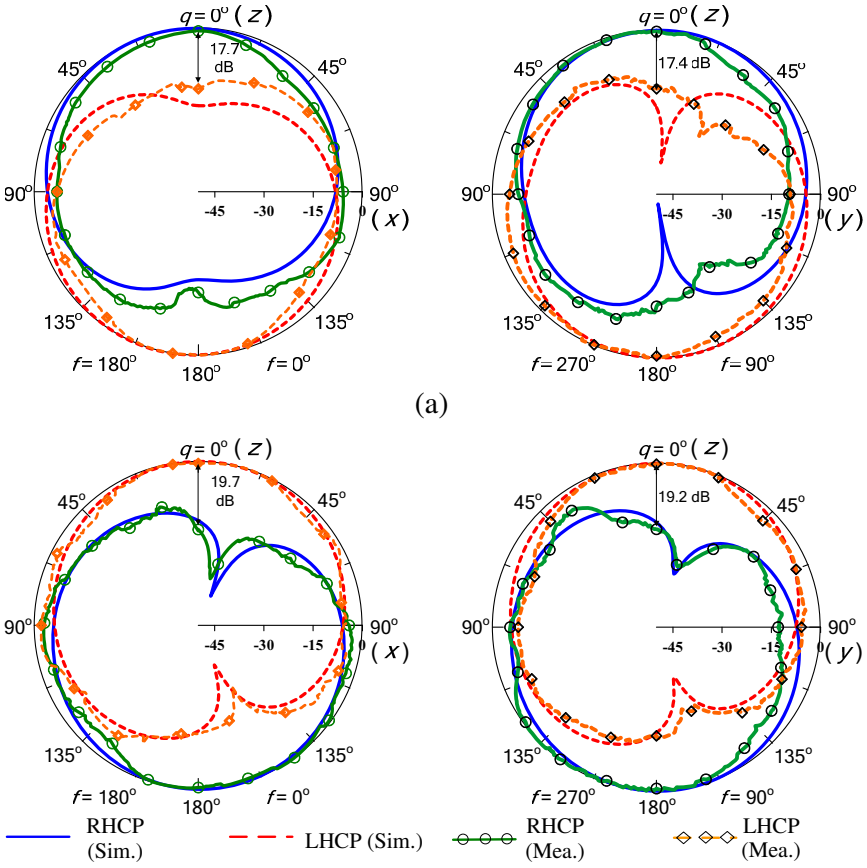

(b)

Figure 10. Simulated and measured normalized RHCP and LHCP radiation patterns at 1.57 and 2.33 GHz. The simulated results (blue solid line and red dashed line) show good agreement with the measured values (green line and orange line with symbols). (a) 1.57 GHz. (b) 2.33 GHz.

systems. Because of the radiation by the resonant path of the fundamental modes, the patterns in these figures are similar. Fig. 10 depicts the normalized CP radiation patterns at 1.57 and 2.33 GHz for the GPS and SDAR systems, respectively. The polarization of the proposed monopole antenna is

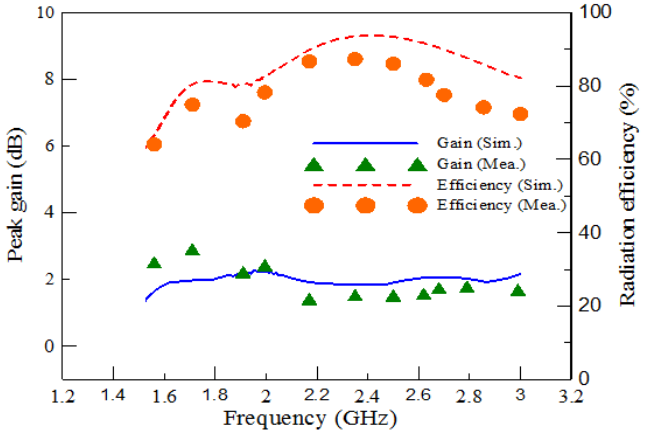

Figure 11. Gain and radiation efficiency of the proposed monopole antenna.

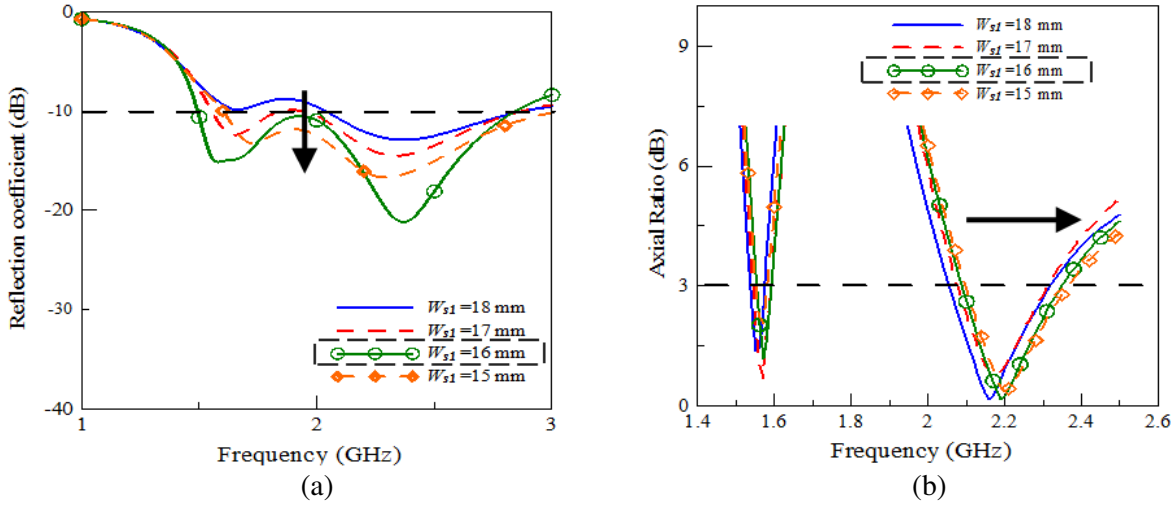

Figure 12. Dependence of the reflection coefficient and axial ratio on W_{s1}. (a) Reflection coefficient. (b) Axial ratio.

right-hand at 1.57 GHz and left-hand at 2.33 GHz. At the GPS band, the power differences between the RHCP and LHCP patterns in the xz- and yz-planes are 17.7 and 17.4 dB. The differences in the xz- and yz-planes are 19.7 and 19.2 dB at the SDAR band, respectively. The power-difference error in the $+z$-axis is caused by the misalignment of the tested antenna when measured in the xz- and yz-planes. Fig. 11 presents a comparison of the peak gain and radiation efficiency of the proposed antenna across the operated frequency band. The average gains in the measurement and simulation for the band are higher than 1.3 dBi. The radiation efficiencies are 62.4% and 88.3% at 1.5 GHz and 3.0 GHz, respectively. The measured and simulated results agree well.

In order to understand the effect of the ground plane on antenna performance, the parametric study has been shown. The parametric results in Figs. 12 and 13 illustrate how the ground plane affects the antenna performance. Fig. 12 shows the dependence of the reflection coefficient and axial ratio on the width (W_{s1}) of the right side of the ground plane. The impedance-matching condition improves when W_{s1} decreases. However, the operated bandwidth becomes narrow. As shown in Fig. 12(b), the CP center frequency around 2.3 GHz slightly moves up with a smaller W_{s1}. With the previous discussion in Fig. 8, the excitation of the circular polarization around 2.21 GHz is partly achieved by the quasi dipole, which is a composite of the short prong and the left ground plane (W_{s1}). The frequency shift of the upper resonance contributes to the variation of the CP frequency around 2.3 GHz. However, the

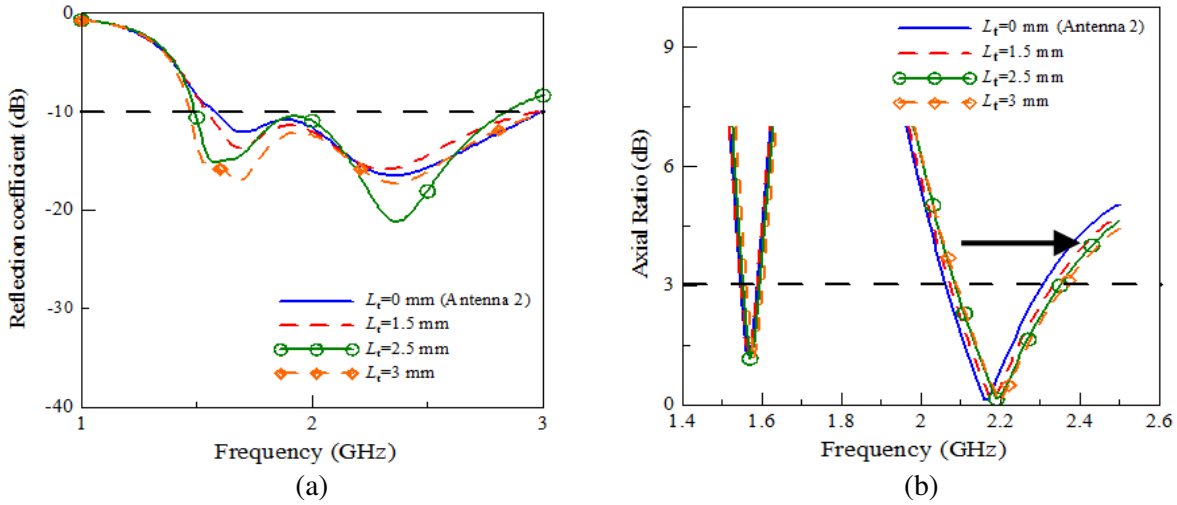

Figure 13. Effects of adjusting L_t on the reflection coefficient and axial ratio. (a) Reflection coefficient. (b) Axial ratio.

circular polarization still excites well. Fig. 13 depicts the effects of the length (L_t) of the stub added at the left side of the ground plane. In Fig. 13(a), the first resonance around 1.57 GHz shifts down because of an increase in the length of the stub. In addition, the impedance-matching condition at the first frequency band also improves as L_t increases. In Fig. 13(b), the CP frequency around 2.33 GHz slightly increases with a larger L_t. However, the CP performance is slightly affected if the ground plane is modified. These results are due to the excitation mechanism of the dual-band CP, which is controlled by the fork-like strip monopole rather than the ground plane. It is possible to design the CP type by setting up the locations of the two prongs and the ground plane. For example, an exchange of two sides of the ground plane maybe excites the RHCP at the higher operated frequency. However, the CP frequency will be tuned by varying the geometric parameters of the prongs and the ground plane. Embedding the proposed antenna inside handsets, notebook computers, and tablets will be convenient for handset designers.

4. CONCLUSION

A design for a CPW-fed fork-shaped antenna with bandwidth enhancement and dual-band circular polarization is demonstrated. The design employs a two-prong topology to excite the CP at the GPS band. In addition, the modification of the ground plane is applied to CP excitation at the SDAR band. Compared with the previous works about the dual-band CP for the microstrip monopole antenna, the design of the proposed antenna possesses the advantages of small size, easily frequency-selective capability, wide impedance bandwidth, and circular polarization. The stable and acceptable radiation characteristics also make the proposed antenna a candidate of a radiating element for integration of multiple wireless communication systems.

REFERENCES

1. Nasimuddin, Z. N. Chen, and X. Qing, "Dual-band circularly polarized S-shaped slotted patch antenna with a small frequency-ratio," *IEEE Trans. Antennas and Propag.*, Vol. 58, No. 6, 2112–2115, Jun. 2010.
2. Wang, C. J., M. H. Shih, and L. T. Chen, "A wideband open-slot antenna with dual-band circular polarization," *IEEE Antennas Wireless Propag. Lett.*, Vol. 14, 1306–1309, 2015.
3. Bao, X. L. and M. J. Ammann, "Monofilar spiral slot antenna for dual-frequency dual-sense circular polarization," *IEEE Trans. Antennas and Propag.*, Vol. 59, No. 8, 3061–3065, Aug. 2011.

4. Weng, W. C., J. Y. Sze, and C. F. Chen, "A dual-broadband circularly polarized slot antenna for WLAN applications," *IEEE Trans. Antennas and Propag.*, Vol. 62, No. 5, 2837–2841, May 2014.
5. Chen, H. D. and H. T. Chen, "A CPW-fed dual-frequency monopole antenna," *IEEE Trans. Antennas and Propag.*, Vol. 52, No. 4, 978–982, Apr. 2004.
6. Liu, W. C., "Wideband dual-frequency double inverted-L CPW-fed monopole antenna for WLAN application," *IEE Proc. — Microw. Antennas Propag.*, Vol. 152, No. 6, 505–510, 2005.
7. Kim, J. I. and Y. Jee, "Design of ultrawideband coplanar waveguide-fed LI-shaped planar monopole antenna," *IEEE Antennas Wireless Propag. Lett.*, Vol. 6, 383–387, 2007.
8. Chang, C. H. and K. L. Wong, "Internal coupled-fed shorted monopole antenna for GSM850/900/1800/1900/UMTS operation in the laptop computer," *IEEE Trans. Antennas and Propag.*, Vol. 56, No. 11, 3600–3604, Nov. 2008.
9. Wang, C. J. and Y. C. Lin, "New CPW-fed monopole antennas with both linear and circular polarisations," *IET Microw. Antennas Propag.*, Vol. 2, No. 5, 466–472, Aug. 2008.
10. Wang, C. J., "A wideband loop-like monopole antenna with circular polarization," *Microw. Opt. Technol. Lett.*, Vol. 53, No. 11, 2556–2560, Nov. 2011.
11. Zhang, L., Y. C. Jiao, Y. Ding, B. Chen, and Z. B. Weng, "CPW-fed broadband circularly polarized planar monopole antenna with improved ground-plane structure," *IEEE Trans. Antennas and Propag.*, Vol. 61, No. 9, 4824–4828, Sep. 2013.
12. Wang, C. J. and K. L. Hsiao, "CPW-Fed monopole antenna for multiple system integration," *IEEE Trans. Antennas and Propag.*, Vol. 62, No. 2, 1007–1011, Feb. 2014.
13. Jou, C. F., J. W. Wu, and C. J. Wang, "Novel broadband monopole antennas with dual-band circular polarization," *IEEE Trans. Antennas and Propag.*, Vol. 57, No. 4, 1207–1034, Apr. 2009.
14. Lu, J. H. and C. W. Liou, "Planar dual-band circular polarization monopole antenna for wireless local area networks," *IEEE Antennas Wireless Propag. Lett.*, Vol. 14, 478–481, 2015.
15. Bor, S. S., T. Lu, J. C. Liu, and B. H. Zeng, "Fractal monopole-like antenna with series Hilbert-curves for WLAN dual-band and circular polarization applications," *Microw. Opt. Technol. Lett.*, Vol. 51, No. 4, 876–880, 2009.
16. Rezaeieh, S. A., "Dual band dual sense circularly polarised monopole antenna for GPS and WLAN applications," *Electron. Lett.*, Vol. 47, No. 22, 1212–1214, Oct. 2011.